

Estimation of offsets in GPS time-series and application to the detection of earthquake deformation in the far-field

J.-P. Montillet,^{1,2} S. D. P. Williams,³ A. Koulali¹ and S. C. McClusky¹

¹Research School of Earth Sciences, The Australian National University, Canberra, ACT 0200, Australia. E-mail: jeanfi_montillet@yahoo.fr

²Cascadia Hazards Institute, Central Washington University, Ellensburg, WA 98926-7418, USA

³National Oceanography Centre, Liverpool, Joseph Proudman Building, 6 Brownlow Street, Liverpool, L35DA, United Kingdom

Accepted 2014 December 8. Received 2014 December 6; in original form 2014 May 12

SUMMARY

Extracting geophysical signals from Global Positioning System (GPS) coordinate time-series is a well-established practice that has led to great insights into how the Earth deforms. Often small discontinuities are found in such time-series and are traceable to either broad-scale deformation (i.e. earthquakes) or discontinuities due to equipment changes and/or failures. Estimating these offsets accurately enables the identification of coseismic deformation estimates in the former case, and the removal of unwanted signals in the latter case which then allows tectonic rates to be estimated more accurately. We develop a method to estimate accurately discontinuities in time series of GPS positions at specified epochs, based on a so-called ‘offset series’. The offset series are obtained by varying the amount of GPS data before and after an event while estimating the offset. Two methods, a mean and a weighted mean method, are then investigated to produce the estimated discontinuity from the offset series. The mean method estimates coseismic offsets without making assumptions about geophysical processes that may be present in the data (i.e. tectonic rate, seasonal variations), whereas the weighted mean method includes estimating coseismic offsets with a model of these processes. We investigate which approach is the most appropriate given certain lengths of available data and noise within the time-series themselves. For the Sumatra–Andaman event, with 4.5 yr of pre-event data, we show that between 2 and 3 yr of post-event data are required to produce accurate offset estimates with the weighted mean method. With less data, the mean method should be used, but the uncertainties of the estimated discontinuity are larger.

Key words: Time-series analysis; Satellite geodesy; Plate motions; Earthquake source observations.

1 INTRODUCTION

For the past few decades, time-series of positions derived from space-geodetic analyses have been used to investigate crustal deformation processes on Earth. Global Positioning System (GPS) time-series have been used to study glacial isostatic adjustment (e.g. Milne *et al.* 2001), hydrological loading (e.g. Bevis *et al.* 2002; Tregoning *et al.* 2009) and pre-, co- and post-seismic earthquake deformation (e.g. Bürgmann *et al.* 2002; Williams 2003b). However, the estimation of geophysical signals such as uplift rates and seasonal loading signals are affected by discontinuities in the GPS time-series that can be caused by equipment changes at individual stations as well as earthquakes causing spatially coherent offsets (e.g. Wdowinski *et al.* 1997; Williams 2003a; Williams *et al.* 2004).

It is well known that the estimation of linear rates of motion (velocities) from time-series of positions are biased in the presence of discontinuities and many different approaches to the estimation

of such offsets have been proposed previously (e.g. Gazeaux *et al.* 2013). Many such studies focus on the identification of offsets under the assumption that the timing of offsets is unknown. For offsets caused by equipment changes (e.g. the replacement of a receiver, antenna or even the disconnection and reconnection of an antenna cable), analysts are totally dependent on site operators to record all events that may affect the estimation of the site location. On the other hand, analysts know with great confidence the timing of discontinuities caused by earthquake deformation. In the former case, offsets are essentially nuisance parameters that must be removed from the GPS time-series in order to estimate geophysical signals (such as interseismic velocities), whereas the offsets themselves are a geophysical signal in the latter case. In both cases, the extent to which the offsets can be estimated affects the accuracy of any subsequent geophysical analysis.

Great earthquakes such as the Sumatra–Andaman event of 2004 December 26 (Banerjee *et al.* 2005) are associated with a number of geodynamic processes occurring over a wide range of spatial and

temporal scales including coseismic strong motion and permanent displacements, free oscillations of the solid Earth and, if located in oceanic regions, tsunamis. In addition, the redistribution of water masses in the ocean due to tsunamis induces further perturbations of the Earth's surface and gravity field (Plag *et al.* 2006). GPS-based studies of seismic displacements from the rupture process of great earthquakes and the associated processes have provided information on the large-scale deformation field, including permanent coseismic offsets, post-seismic non-linear displacements and the tsunami-induced loading signal (Banerjee *et al.* 2005; Khan & Gudmundsson 2005; Kreemer *et al.* 2006a). In order to estimate coseismic offsets, time-series of weekly, daily or subdaily GPS coordinate estimates are generated from networks of GPS stations. These time-series contain interseismic strain information, coseismic displacements and post-seismic relaxations as well as seasonal signals and unmodelled orbital errors. In this study we focus on the ability to estimate coseismic offsets from GPS stations in the far-field of large earthquakes. Events with magnitude $M_w > 9.0$, create displacements over a large part (or all) of the globe. Previous studies, for example Banerjee *et al.* (2005) and Tregoning *et al.* (2013), estimated millimetre-level coseismic offsets at GPS stations thousands of kilometres from earthquake ruptures. For the Sumatra–Andaman earthquake ($M_w > 9.0$), the earthquake ruptured about 1300 km of the Sunda and Andaman subduction zone (Pollitz *et al.* 2006; Banerjee *et al.* 2007).

Banerjee *et al.* (2007) showed that GPS stations close to the ruptured subduction zone underwent vigorous post-seismic relaxation in the years following this event, while Watson *et al.* (2010) and Tregoning *et al.* (2013) showed post-seismic relaxation effects in South Australia following the December 2004 Macquarie Ridge earthquake. Thus, the estimation of a discontinuity in a GPS time-series is more complicated when caused by an earthquake than in the case of an equipment change because of the possible presence of post-seismic non-linear signals, even thousands of kilometres from the earthquake rupture. Historically, two different approaches have been used to estimate such coseismic offsets involving either estimating the difference between mean coordinate values of short sections of data before/after an earthquake or more sophisticated modelling of site motion that includes linear motion, seasonal signals and the coseismic offsets. In a study of the Landers earthquake in South California (1992 June 28), 100 d (in total) of GPS data were used to calculate coseismic offsets (Wdowinski *et al.* 1997). For the study of the co- and post-seismic signals of the Nias earthquake (2005 March 28), Kreemer *et al.* (2006b) used 180 d. Chen *et al.* (2004) estimated coseismic offsets arising from 2002 March 31 Taiwan earthquake (at Hualien) using 18 months of data. Boschi *et al.* (2006) used time-series from 2 to 9.5 yr of continuous data to produce the displacement field of the Sumatra–Andaman Earthquake.

In these studies, the length of the GPS coordinate time-series was selected based on some *a priori* assumptions on the statistics and geophysical processes embedded in the GPS coordinate time-series. GPS coordinate time-series are generally modelled as a sum of seasonal variations, noise (e.g. white noise, flicker noise and random-walk), the presence (or absence) of post-seismic relaxation and tectonic rate (Williams *et al.* 2004). For example, some studies take into account the post-seismic relaxation occurring at some GPS stations by either fitting a logarithmic model to the post-seismic coordinate time-series using 180 d of data (Kreemer *et al.* 2006b), or a straight line using 18 d before and 9 d after the event (e.g. Banerjee *et al.* 2007). Studies such as Banerjee *et al.* (2005) and Watson *et al.* (2010) justify the use of a very short window

length (respectively 5 and 7 d) as a compromise in minimizing biases caused by daily variability, longer period time-correlated noise and post-seismic relaxation. To the contrary, long time-series are used in order to average the effect of stochastic and geophysical processes (i.e. coloured noise, seasonal variations), or to minimize the bias of removing the tectonic rate which affects the accuracy of coseismic offset estimates (Boschi *et al.* 2006).

This work investigates different approaches for estimating coseismic deformation. We consider the effect of different window lengths of data, the presence (or absence) of noise, seasonal variations, tectonic motion and post-seismic relaxation. We assess the effectiveness of different models of site motion, given different window lengths, for resolving coseismic offsets and which models work best given certain levels of noise and data availability. We describe an algorithm that calculates a coseismic offset of a given event based on no *a priori* assumptions about the statistics of the GPS coordinate time-series. The final goal is to provide precise and accurate coseismic offset estimates for GPS time-series from stations located in the far-field of a given event (with a distance ≥ 1000 km). The following sections describe our approach using simulated and real GPS time-series.

2 ESTIMATING OFFSETS: HYPOTHESIS AND METHODOLOGY

Given a GPS coordinate time-series, it should be possible to estimate accurately an offset at a nominated time in the absence of any stochastic processes (i.e. noise). However, actual GPS time-series are a sum of stochastic processes and other signals caused by, for example, seasonal variations, satellite orbit errors and other insufficiently modelled processes (Williams 2003b). These stochastic processes contained in the GPS coordinate time-series, plus possible biases due to other offsets occurring within the same time frame of the selected GPS data, may affect the accuracy of the offset estimate because the processes are difficult to model. Therefore, the aim of this paper is to derive an accurate and precise offset from a given amount of data with little information about the characteristics of the different geophysical processes (i.e. amplitude of the noise, amplitude of the seasonal variations) embedded in the GPS time-series. The philosophy applies to offsets caused by any process, but in this paper we focus on offsets caused by coseismic displacements.

The results shown in this work assume that the time-series have had an *a priori* tectonic rate removed and therefore only a residual rate may remain. This bias of detrending the time-series is included in the total error of the estimated coseismic offsets and is denoted below as tectonic rate error. However, we do not investigate specifically the bias due to the estimation of a coseismic offset within GPS time-series as a function of the amplitude of the tectonic rate. Williams (2003a) dealt with this issue.

In the following section, we define a 'coseismic offset series' using simulated time-series. Section 2.2 describes the different ways of simulating GPS coordinate time-series, or inserting known offsets into actual GPS coordinate time-series. Finally, Section 2.3 focuses on two methods to produce a coseismic offset series, and the algorithms to estimate the final coseismic offset from those series.

2.1 Coseismic offset series: definition and examples

We simulate a GPS coordinate time-series with almost no noise (amplitude of white noise, $A_{wh} = 0.01$ mm, amplitude of coloured

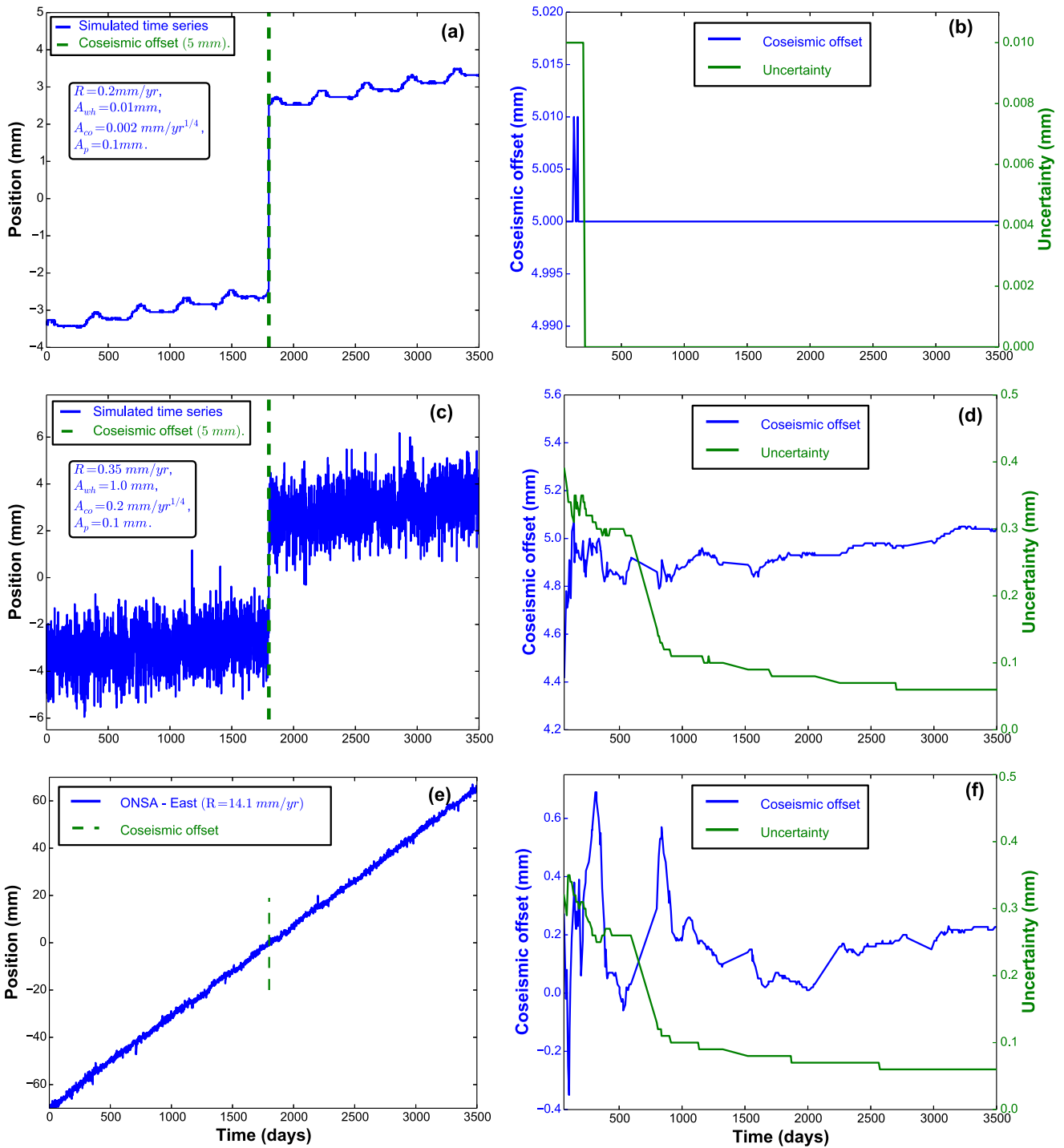


Figure 1. Panels (a) and (c): simulated GPS coordinate time-series (A_{wh} amplitude of white noise, A_{co} amplitude coloured noise, A_p amplitude of the periodic signals, R tectonic rate); panels (b) and (d): corresponding coseismic offset series; panels (e) and (f): east coordinate time-series for *ONSA* GPS station with corresponding coseismic offset series.

noise, $A_{co} = 0.002 \text{ mm yr}^{-1/4}$, a step function of 5 mm representing a coseismic offset, an annual (and semi-annual) periodic signal (amplitude, $A_p = 0.1 \text{ mm}$) to represent seasonal variations (Fig. 1a), and with a small tectonic rate error (0.2 mm yr^{-1}). In this study, the amplitude of the coloured noise is simulated following Williams *et al.* (2004) and Montillet *et al.* (2013b). We estimate the coseismic offset using different window lengths of data centred on the date of the nominated event. This results in what we call a ‘coseismic

offset series’, as shown in Fig. 1(b). In this ideal case, the coseismic offset series is almost a straight line with a mean value equal to the true value of the coseismic offset. The x -axis of the coseismic offset series (Dt in days) displays the total amount of data (the amount of data before and after the event are the same) used to calculate each coseismic offset.

We now increase the amplitude of noise ($A_{wh} = 1 \text{ mm}$, $A_{co} = 0.2 \text{ mm yr}^{-1/4}$) and tectonic rate error (Fig. 1c). The

amplitude of the seasonal signal remains the same. The associated coseismic offset series (Fig. 1d) is no longer a straight line. Rather, it converges to the true coseismic offset value when the length of the GPS time-series is greater than 1800 d, that is 5 yr.

Finally, we use the east component of a real GPS time-series (*ONSA*—Onsala station; Fig. 1e) with a time span from 2000 March to 2010 January, and compute the associated coseismic offset series evaluated at the date of the Sumatra–Andaman event (Fig. 1f). The fluctuations in the coseismic offset series using real data are more random. This highlights the challenge of estimating a precise coseismic offset from GPS time-series in the far-field of an event containing actual noise and geophysical signals. Note that we chose *ONSA* as an example of a time-series that is known to be unaffected by many large earthquakes and other discontinuities (i.e. antenna offsets). This makes it an ideal case for estimating the coseismic offset series from the real time-series.

2.2 Simulated coseismic offset in real GPS coordinate time-series

For a more realistic scenario of the actual noise in the GPS time-series, we inserted offsets into actual GPS time-series containing real geophysical signals and stochastic processes. For this purpose, we selected GPS stations (e.g. *ONSA*) that do not contain post-seismic relaxation signals, are not contaminated by many earthquakes or instrument related discontinuities and are located in the far-field of the great Sumatra–Andaman 2004 earthquake (Kreemer *et al.* 2006a). We then insert a known coseismic offset at some specific time. In these simulations, the time of the simulated event corresponds to the Sumatra–Andaman earthquake (2004 December 26). We vary the amount of data available after the event to investigate the effects of time-series length on the accuracy of the desired coseismic offset.

2.3 Methodology to estimate a coseismic offset and resulting coseismic offset series

The choice of the method to estimate the coseismic offset with the best accuracy and precision, depends on the amount of available data. For a sufficiently small amount of data, it is most likely that the noise dominates over the other geophysical processes. When increasing the amount of data, we gradually have to take into account tectonic rate errors and periodic variations.

In order to produce the coseismic offset series, we develop two ways of calculating the coseismic offsets for a given GPS coordinate time-series. A simple method (or mean method) consists of averaging coordinates immediately preceding and following the day of a nominated event, and then subtracting the mean values from each other. A full method uses the least-squares technique with a complete site motion model, including a linear trend and/or seasonal variations, to describe the coordinate time-series.

To test the procedures, we start with a formula for the full method with the functional model including linear trend and seasonal variations. Consider the linear equation for a times-series, y_i , where there is one offset at time, t_{off} ($t_0 < t_{\text{off}} < t_{N-1}$), with N the number of samples in the nominated time-series.

$$y_i = y_0 + r t_i + o p_i + \varepsilon(t_i), \quad (1)$$

where $\varepsilon(t_i)$ is the error term and p_i is the Heaviside function ($p_i = 1$ if $t_i \geq t_{\text{off}}$). Using the same methodology proposed by Blewitt & Lavallée (2002) for deriving the velocity bias due to neglecting a

periodic signal, one can estimate the total offset bias of the estimates $\hat{\mathbf{v}} = (\hat{y}_0, \hat{r}, \hat{o})^T$. The offset bias error with the full method when using the model of site motion, including linear trend and annual signal, is given by:

$$\sigma_{\hat{o}(\text{wh})} \approx \sqrt{\frac{16\sigma_{\text{wh}}^2 \Delta T}{T}} \quad (2)$$

which is similar to the equation of Williams (2003b), but our formula is for the case of white noise only. The full derivation is given in Appendix A. Now if $y(t)$ is some function that we have failed to take into account, it will then produce a bias in the estimates $\hat{\mathbf{v}}$. By introducing the signal $f(t) = a \cos(2\pi f t - \phi)$ in the derivation, one can then obtain the offset bias formula (see Appendix A):

$$\sigma_{\hat{o}}(T) = \frac{2a}{(\pi T f)^2} \left\{ 9 - 9 \cos(2\pi T f) - 6\pi T f [4 \sin(\pi T f) + \sin(2\pi T f)] + 2(\pi T f)^2 [\cos(\pi T f + 2)]^2 \right\}^{1/2} \quad (3)$$

Reusing the same methodology, it is also possible to account for a bias introduced due to a post-seismic relaxation mechanism, $y_p(t, \tau) = B(1 - \exp(-\frac{t}{\tau}))$ (t is in $[\frac{T}{2}, T]$, and τ is the relaxation time). Following the derivation given in Appendix A, the bias formula is then:

$$\begin{aligned} L_1(T, \tau) &= B \left[\frac{T}{2} + \tau \exp\left(-\frac{T}{\tau}\right) \left(1 - \exp\left(\frac{T}{2\tau}\right)\right) \right] \\ L_2(T, \tau) &= B \left[\frac{3T^2}{8} + \tau T \exp\left(-\frac{T}{\tau}\right) \left(1 - \frac{1}{2} \exp\left(\frac{T}{2\tau}\right)\right) \right. \\ &\quad \left. + \tau^2 \exp\left(-\frac{T}{\tau}\right) \left(1 - \exp\left(\frac{T}{2\tau}\right)\right) \right] \\ \sigma_{\hat{o}_p}(T, \tau) &= \frac{20}{T} L_1(T, \tau) - \frac{24}{T^2} L_2(T, \tau). \end{aligned} \quad (4)$$

Finally when including only the tectonic rate in the functional model, the offset bias error is the square root of the quadratic sum of the eqs (2), (3) and (4). If the functional model includes the tectonic rate and a post-seismic relaxation model, the offset bias error is equal to eq. (3).

We can apply a similar methodology to above when we use the mean method instead of the full method to estimate the offset. We estimate two means of length $T/2$ either side of the offset which can give the estimate of the offset bias $\sigma_{\hat{o}_2}$:

$$\begin{aligned} \sigma_{\hat{o}_2} &= \sigma_1(T) + \sigma_2(T) + \sigma_3(T, \tau) \\ \sigma_1(T) &= \frac{rT}{2} \\ \sigma_2(T) &= \frac{8^{1/2} a \sin\left(\frac{\pi T f}{2}\right)^2}{\pi T f} \\ \sigma_3(T, \tau) &= B \left[1 + \frac{2\tau}{T} \exp\left(-\frac{T}{\tau}\right) \left(1 - \exp\left(\frac{T}{2\tau}\right)\right) \right]. \end{aligned} \quad (5)$$

Appendix A gives some details on how to derive eq. (5). For the bias introduced in the case of the white noise, we refer to the estimation in Williams (2003b). Finally, the offset bias for the mean method introduced with the linear trend, seasonal variations and white noise is the square root of the quadratic sum of σ_1 , σ_2 , σ_3 and $\sigma_{\hat{o}(\text{wh})}$.

We now estimate the coseismic offset bias for the mean method and the full method when using different parameters, in order to study the way the two methods operate. The results for different values of the tectonic rate and amplitude of the seasonal variations

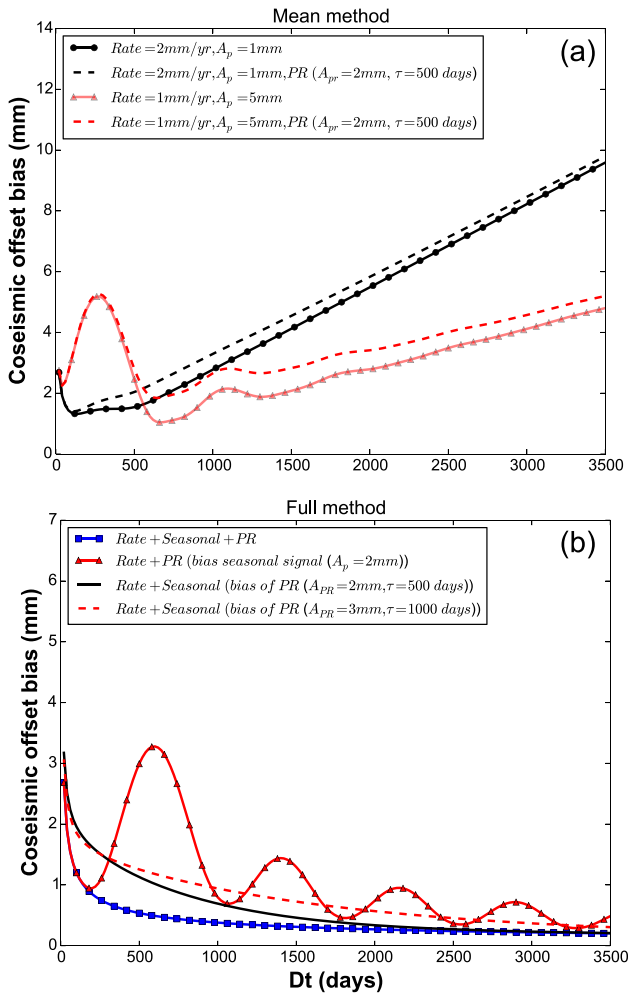


Figure 2. (a) Coseismic offset bias for different tectonic rates (*Rate*), different amplitudes of seasonal signal (A_p) and varying the parameters in the post-seismic relaxation phenomenon (amplitude A_{PR} , relaxation time τ) using the Mean method; (b) Coseismic offset bias with various functional model in the full method [linear trend (*Rate*), seasonal signal (*Seasonal*), post-seismic relaxation model (*PR*)].

are displayed in Figs 2(a) and (b). The amplitude of the noise is fixed to 3 mm for all the results.

Fig. 2(a) shows the coseismic offset bias series corresponding to the mean method, which generally have three characteristic regions. In the first part ($Dt < 480$ d), the amplitude of the noise and the amplitude of the seasonal signal are most likely the main sources of error affecting the accuracy of the estimated coseismic offset. Then there is a short interval which resembles an inflection point ($480 < Dt < 700$ d) where the error caused by the noise and seasonal signals is minimal. In the last part of the series, the estimated coseismic offsets are increasingly biased by the tectonic rate error. Note that when the amplitude of the seasonal signal is small ($A_p = 1 \text{ mm yr}^{-1}$), the inflection point appears around 500 d, whereas when the amplitude of the seasonal signal is large the inflection point appears later on (650–700 d). In addition when adding a post-seismic relaxation signal (i.e. duration $\tau = 500$ d, amplitude $A_{PR} = 2 \text{ mm}$), the results show that the bias error to the true value of the offset increases at the inflection point, and it also increases the time interval before the tectonic rate starts dominating the bias error in the estimated offset.

Fig. 2(b) displays the results of the coseismic offset bias series produced by the full method using eqs (2)–(4). The functional model always includes the tectonic rate (*Rate*). Depending on the scenario, the seasonal signal (*Seasonal*) and/or the post-seismic relaxation model (*PR*) are included. When taking into account all these geophysical processes (*Rate* + *Seasonal* + *PR*), the remaining bias is due to the white noise. Note that if no post-seismic relaxation phenomenon was experienced in the time-series, the results will be reduced to the first two curves (*Rate* + *Seasonal* + *PR*, *Rate* + *PR*). Without post-seismic relaxation (or completely accounted for in the functional model), the first two curves show an asymptotic behaviour after approximately 100–1500 d. The results corresponding to *Rate* + *Seasonal* + *PR* converge to an error smaller than 1 mm after 100 d. Thus, the smaller the amplitude of the seasonal signal the sooner the asymptotic behaviour appears. In addition, the results show that it takes longer time-series to get the asymptotic part close to the true value of the offset when not accounting for a post-seismic relaxation mechanism (see last two curves—*Rate* + *Seasonal*). Note that we do not use the full method to estimate any coseismic offset if the amount of GPS data is less than 60 d (30 d before and 30 d after) in this scenario and all the following scenarios, because there is not enough data to estimate all the parameters in the model.

Looking at the coseismic offset bias series associated with the mean method, precise estimates are found at the inflection point in a selected interval (Mahnke *et al.* 2008). Simulations show that it is difficult to find exactly this inflection point, but it is possible to calculate an upper bound of the interval where the inflection point should lie (if it exists). We formulate a hypothesis that the optimum interval corresponds to when the variance of the noise is greater than or equal to the variance of the time-series around a mean value without accounting for the tectonic rate error. However, the optimum window may be very short if the variance of the noise is very small or for a large tectonic rate error. In contrast, the optimum window may be greater than 1 yr for a small tectonic rate error ($< 3 \text{ mm yr}^{-1}$) and a total noise amplitude (white and coloured noise) less than 5 mm. Averaging the coseismic offset over several years may be unrealistic in the case of real time-series, since a large number of events occurring during such period may affect the accuracy of the coseismic offset estimate (e.g. repetitive events affecting GPS stations close to the San Andreas fault (Wdowinski *et al.* 1997).

Furthermore in Fig. 2(b), the values of the coseismic offset estimated with the full method and short observation window, have large offset biases. This is the period where there are barely enough data to calculate the parameters of the full model. During this time interval ($Dt < 100$ d for *Rate* + *Seasonal* + *PR* (first curve -blue), $Dt \leq 1000$ d for *Rate* + *PR* only (second curve)), the mean and full method can yield similar results with large uncertainties. In order to derive a precise and accurate estimate of the coseismic offset with the mean method, one has to look at the coseismic offset series to detect any inflection points and find the optimum window. If no inflection point can be found or the optimum window is greater than a year, we choose to estimate the coseismic offset by averaging the coseismic offset series with a maximum amount of data equal to 100 d (50 d before and after the event) unless otherwise stated.

Figs 2(a) and (b) show how the coseismic offset series will behave with longer and longer time-series and given the amplitude of noise, seasonal signal, post-seismic relaxation mechanism and tectonic rate error. However, one can assume a similar behaviour of the offset bias error associated with the estimated coseismic offsets, as shown in Fig. 1. Looking at the coseismic offset series associated with the full method, all points of the coseismic offset series with same order of magnitude of the uncertainties should be considered

as precise estimates of the coseismic offset without any *a priori* knowledge of the true value of the coseismic offset. We derive our final estimate of the coseismic offset by calculating the weighted mean of the entire coseismic offset series, where the weight of each value in the coseismic series is the uncertainty associated with the coseismic offset estimate for each window length (Larson & Agnew 1991). In the following sections, estimating the coseismic offset by first producing a coseismic offset series with the full method and then calculating the weighted mean to evaluate the estimate will be termed the ‘weighted mean method’.

Note that the uncertainties associated with the mean method are estimated by calculating the root mean square of the observations for each selected window. The uncertainties associated with the weighted mean method are estimated from the covariance matrix assuming that the noise process is a first order Gauss–Markov process. We do this simplification of the noise model compared with a full stochastic model including white noise and flicker noise in order to decrease the computation time (Williams *et al.* 2004).

Finally, including the seasonal signal into the full method yields virtually the same results as not including it when less than 1 yr of data are used (see Fig. 2b). Thus, we always include a seasonal signal in the model of the site motion when estimating a coseismic offset in the remainder of this study.

3 RESULTS AND DISCUSSIONS

3.1 Performances of the two methods using simulated time-series

The GPS time-series are simulated following the two first examples described in Section 2.1. They include white and coloured noise, seasonal variations and tectonic rate. The tectonic rate varies up to 30 mm yr⁻¹. However, the mean method is applied to time-series with residual tectonic rate up to 5 mm yr⁻¹ in order to replicate the error of detrending the time-series before applying this method. We evaluate the performances of the mean method and the weighted mean method through four scenarios as shown in Table 1. In addition, as the simulated GPS time-series span 9.5 yr, it is sometimes relevant for some scenarios to compare the performance of the weighted mean method on short parts of the coseismic offset series. We use a weighted mean short-term strategy (*Weighted Mean SS*) when using a maximum of 1 yr of GPS data (6 months before and following the date of the event), and

Table 1. Parameters used for the simulations with the true amplitude of the coseismic offset for the nominated event (*Coseismic*), the amplitude of the simulated noise components (*Noise*) and the amplitude of the seasonal variations (*Seasonal*). (*h*) means the GRACE elastic deformation signal is used for the seasonal component. (*) indicates that the coloured noise is only the flicker noise component in these simulations, and its amplitude is always smaller than the amplitude of the white noise. [.] means the minimum and maximum value that a parameter can take (randomly) within this interval during the simulations.

Scenario	Coseismic (mm)	Noise		Seasonal (mm)
		White (mm)	Coloured (*) (mm ^{1/4})	
1	5	[0.01,5.6]	[0.002,2.4]	0.1
2a	5	3.5	1.5	[0.01,5.1]
2b	5	3.5	1.5	[0.5,5.1] (h)
3	5	3.2	1.8	1.5

a weighted mean long-term strategy (*Weighted Mean LS*) with a minimum of 7 yr of GPS data (3.5 yr before and following the date of the event). Note that in the following, the *y*-axis of the figures displays the absolute error (absolute difference between the true and estimated coseismic offset) in millimetres, averaged over the results from 40 simulated GPS coordinate time-series, varying randomly the tectonic rate error between 0.1 and 3 mm yr⁻¹ (Monte Carlo simulations). In each simulation, the uncertainties are estimated for each method following Section 2.3. The uncertainties displayed for each following scenario, are an average over all simulations.

In Scenario 1, we vary only the amplitude of the (white and coloured) noise according to the parameters listed in Table 1, having inserted a fixed coseismic offset of 5 mm into the middle of the time-series (at 1734 d). Fig. 3(a) displays the mean error and the associated uncertainties for the two methods, with the *x*-axis showing the square root of the quadratic sum of the amplitude of the two noise components. Note that the amplitude of the noise is defined in the same way for the remainder of the paper. The weighted mean method and the mean method perform comparably (error ≤ 0.5 mm) when the amplitude of the noise is smaller than 2 mm, but the uncertainties of the estimated coseismic offsets are larger for the mean method. To recall Section 2.3, when estimating the coseismic offsets with 100 d of data and a time-series containing a small tectonic rate error, the mean method gives large uncertainties. On the one hand, one could average the final coseismic offset estimate on a smaller coseismic offset series (reducing the maximum amount of data to less than 100 d) in order to decrease the uncertainties, but on the other hand it decreases the accuracy of the coseismic offset estimate. This highlights the great sensitivity of the mean method to the presence of noise. In contrast, the results show that the weighted mean method performs with an error closely bounded by the results of the long-term strategy (*Weighted Mean LS*), with an averaged coseismic offset error less than 0.5 mm for all amplitudes of the noise tested in this scenario.

We now simulate GPS time-series with a fixed amplitude of noise, insert only one coseismic offset, and vary the amplitude of the seasonal signal. The parameters are listed in Scenario 2a in Table 1. The results in Fig. 3(b) show that, for a seasonal variation modelled as a periodic signal with a first and second harmonic ($f_1 = 365$ d and $f_2 = 182.5$ d), the mean error and uncertainties of the weighted mean are small (better than 0.5 mm error with uncertainties of less than 0.4 mm). The coseismic offset series resulting from the weighted mean method is asymptotic and it converges quickly to the true estimate of the coseismic offset, even in the presence of seasonal signals. This is supported when looking at the results given by the long-term strategy (*Weighted Mean LS*): the error values with the weighted mean and the *Weighted Mean LS* are very close. In contrast, the error of the coseismic offset estimated with the mean method shows a strong sensitivity to the amplitude of the seasonal signal. For example, for an amplitude of seasonal variations of 1 mm, the mean error is around 0.5 mm (with associated uncertainties of 1 mm), and at 4 mm the amplitude of the error is approximately 1 mm (with associated uncertainties of 2 mm). As noted in the first case scenario: with a small tectonic rate error the coseismic offset and uncertainties are calculated in this case with the maximum amount of data (100 d). Common knowledge (e.g. Banerjee *et al.* 2007; Watson *et al.* 2010) indicates that the estimation of coseismic offsets from GPS time-series shorter than a few weeks should not be affected by seasonal signals. This does not give any confidence that the seasonal variations are effectively null-averaged using the optimum window or the maximum amount of data. In fact, the

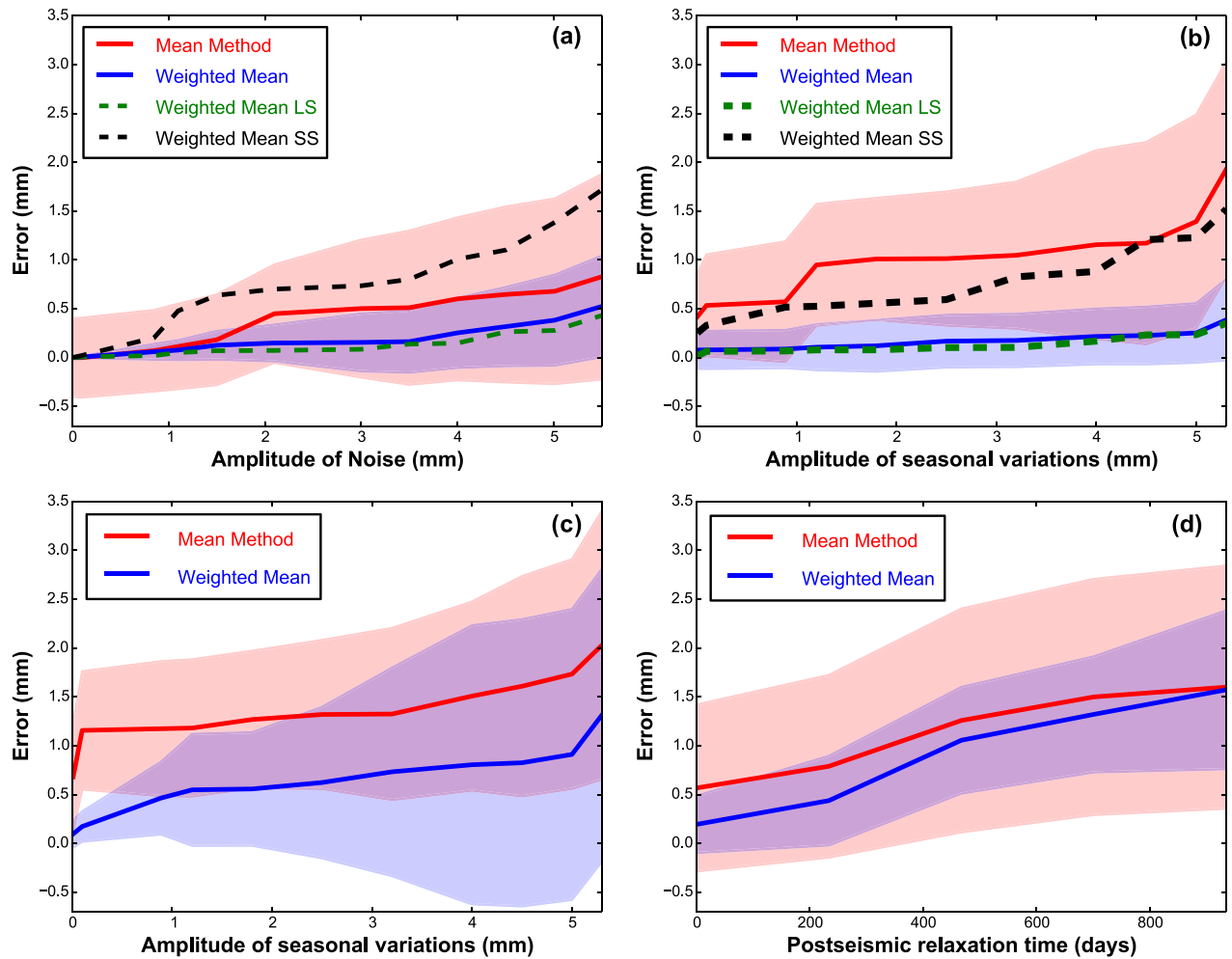


Figure 3. Averaged error bias for mean method and weighted mean method with varying noise (a), amplitude of the seasonal signal (b), amplitude of the GRACE elastic deformation signal (c), and relaxation period as a model of the coseismic offset (d). Shaded areas are associated uncertainties. *LS* and *SS* denote long-term and short-term strategies.

results underline the sensitivity of the mean method to the amplitude of the seasonal variations.

Davis *et al.* (2012) showed that the elastic deformation estimated from GRACE observations can be used as a nonstochastic model in the simulated GPS time-series instead of the periodic model of the seasonal signal used in the previous simulations. Thus, we simulate GPS time-series with parameters similar to Scenario 2a in Table 1, but replace the deterministic model of the seasonal signal with the elastic deformation as derived from GRACE estimates of surface loads (also called GRACE elastic deformation signal) (Darbeheshti *et al.* 2013). This is called Scenario 2b in Table 1. Note that for all simulations, the GRACE elastic deformation signal is calculated for Brazil (Sinop – Mato Grosso), to get a quasi-periodic signal with a large amplitude. This quasi-periodic signal is very similar to the one estimated at BRAZ site displayed in the study of Tregoning *et al.* (2009).

The errors associated with the weighted mean method are much larger than the ones calculated in the previous case (more than 50 percent of the mean error value for the amplitude of the seasonal variations greater than 1 mm). The difference in the results between this scenario and the previous one emphasizes that the quasi-seasonal variations with a non-stochastic model introduce a large bias in the coseismic offsets estimated with the weighted mean

method. This shows the importance of estimating the seasonal signal correctly to obtain an accurate coseismic offset estimate. In addition, the error values associated with the mean method are greater than the ones with the weighted mean method. However, the uncertainties are the same magnitude for an amplitude of the seasonal variations greater than 1 mm. Therefore, in this scenario, the mean method can give similar estimates to the weighted mean method.

Finally, we simulate GPS time-series fixing the amplitude of the noise and the seasonal signal, but inserting a post-seismic relaxation delay according to Scenario 3 in Table 1 (see Fig. 3d). The post-seismic relaxation delay is modelled with a small amplitude (less than 1.5 mm) in order to simulate the case where it is difficult to detect it in the simulated GPS time-series due to other geophysical processes and coloured noise. The results show that the mean method yields coseismic offsets with the largest absolute error and uncertainties. The explanation is similar to the previous scenarios: with relatively small tectonic rate residual in the time-series the coseismic offset and uncertainties are calculated in this case with the maximum amount of data (100 d). When estimating the different coseismic offsets with the weighted mean method, the results show that the weighted mean method is less sensitive to the presence of post-seismic relaxation delays.

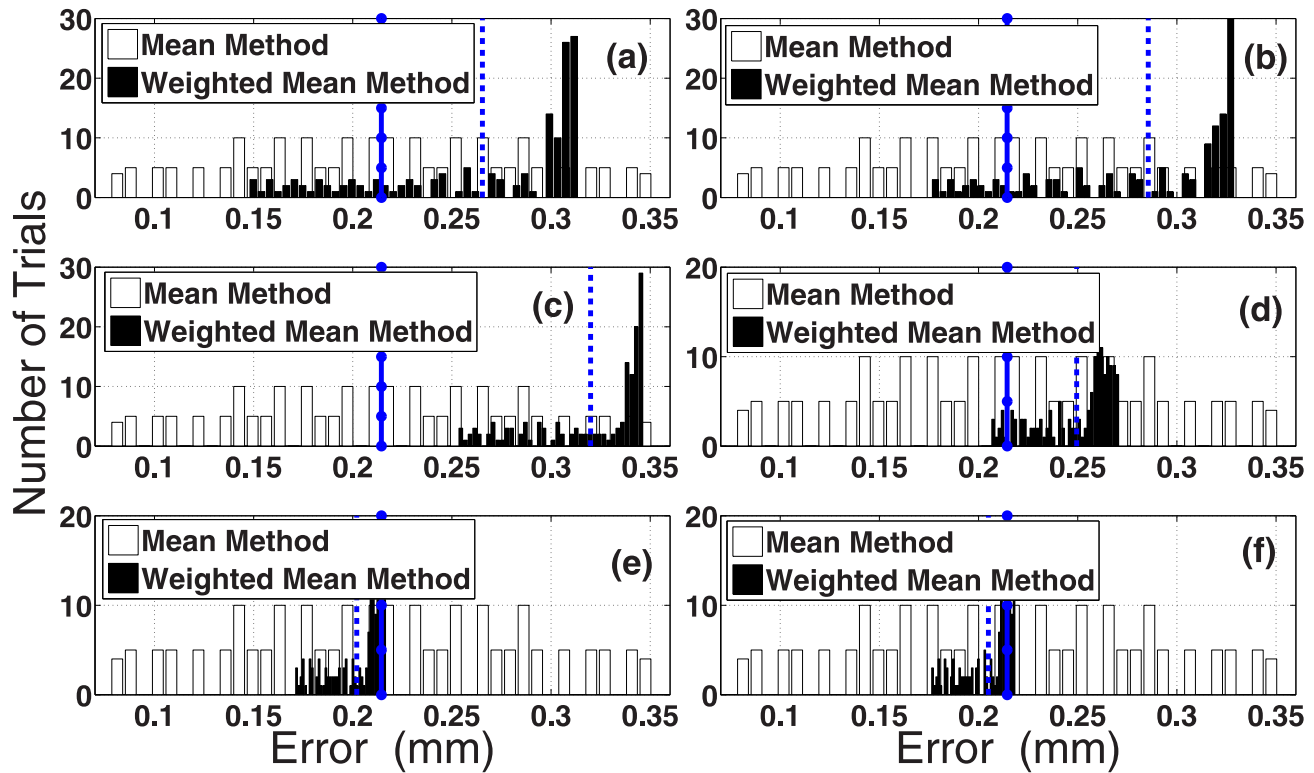


Figure 4. Histogram of the absolute error (in mm) for the mean method and the weighted mean when processing the coseismic series between 6 months and 9 yr [(a) 3 + 3 months, (b) 6 + 6 months, (c) 1 + 1 yr, (d) 1.5 + 1.5 yr, (e) 3 + 3 yr, (f) 4.5 + 4.5 yr]. Note that the (blue) dotted line is the mean value for the Mean method, the (blue) dashed line is the mean value for the Weighted Mean method.

3.2 Performance of the two methods relative to the length of the time-series

3.2.1 Amount of GPS data available and the accuracy of the weighted mean method

In the previous section we showed that, in the case of long GPS coordinate time-series (9 yr) with a simulated coseismic offset inserted in the middle, the weighted mean method performs better in terms of accuracy and precision than the mean method. However, can the mean method outperform the weighted mean method if only a short amount of data are available after an event, such as would be the case if studying an earthquake only weeks after it had happened?

To investigate this, we use real GPS detrended time-series and follow the processing described in Section 2.2 (e.g. noise in the GPS time-series, date of the simulated event). We then simulate 195 GPS time-series changing the amplitude of the inserted coseismic offset (between 1 and 10 mm) and the tectonic rate varies up to 30 mm yr^{-1} . However, the mean method is applied on time-series with residual tectonic rate varying between 0.5 and 3 mm yr^{-1} in order to replicate the error of detrending the time-series before applying this method. In order to avoid any degradation of the coseismic offset estimates with the influence of other events, we set the maximum amount of data equal to 100 d (50 d before and after the event). We then calculate the absolute error between the true coseismic offset and the estimated one using various amount of data. Fig. 4 shows the results in terms of histograms of the absolute error between the true coseismic offset and the estimated value with the two approaches when processing the GPS time-series with window lengths of

6 months (3 + 3 months) to 9 yr (4.5 + 4.5 yr). Note that the statistics for each histogram are displayed in Table B1.

Overall, the results show that the standard deviation of the error computed by the weighted mean method is less than the standard deviation of the results with the mean method with more than 2 yr of GPS time-series. Using 1 or 2 yr, the standard deviation of the error when using the two methods is comparable. However, the mean error is up to 0.32 mm for the weighted mean results with 2 yr or less of GPS data, whereas the mean error of the mean method is equal to 0.21 mm. Thus, the weighted mean method performs slightly worse than the mean method. These results can be explained when looking at the exponential decreasing shape of the uncertainty series described in Section 2.3 (e.g. Fig. 2b). When the uncertainties become asymptotic, it can be assumed that there are enough GPS data to robustly estimate all the parameters of the site motion model (e.g. tectonic rate, seasonal signal). With 3 yr of data (e.g. Fig. 4d), the standard deviation of the results with the weighted mean method is equal to a sixth of the estimated results with the mean method. In addition, the mean error is around 0.25 mm (see Table B1). Thus, one should use the weighted mean method with long GPS time-series ($Dt \geq 3 \text{ yr}$ – or 1.5 yr before and after the time of the event).

3.2.2 Real case scenario: an amount of post-event GPS data available

GPS stations started to be permanently installed to monitor geophysical processes since the mid 1980s. Thus, the estimation of a

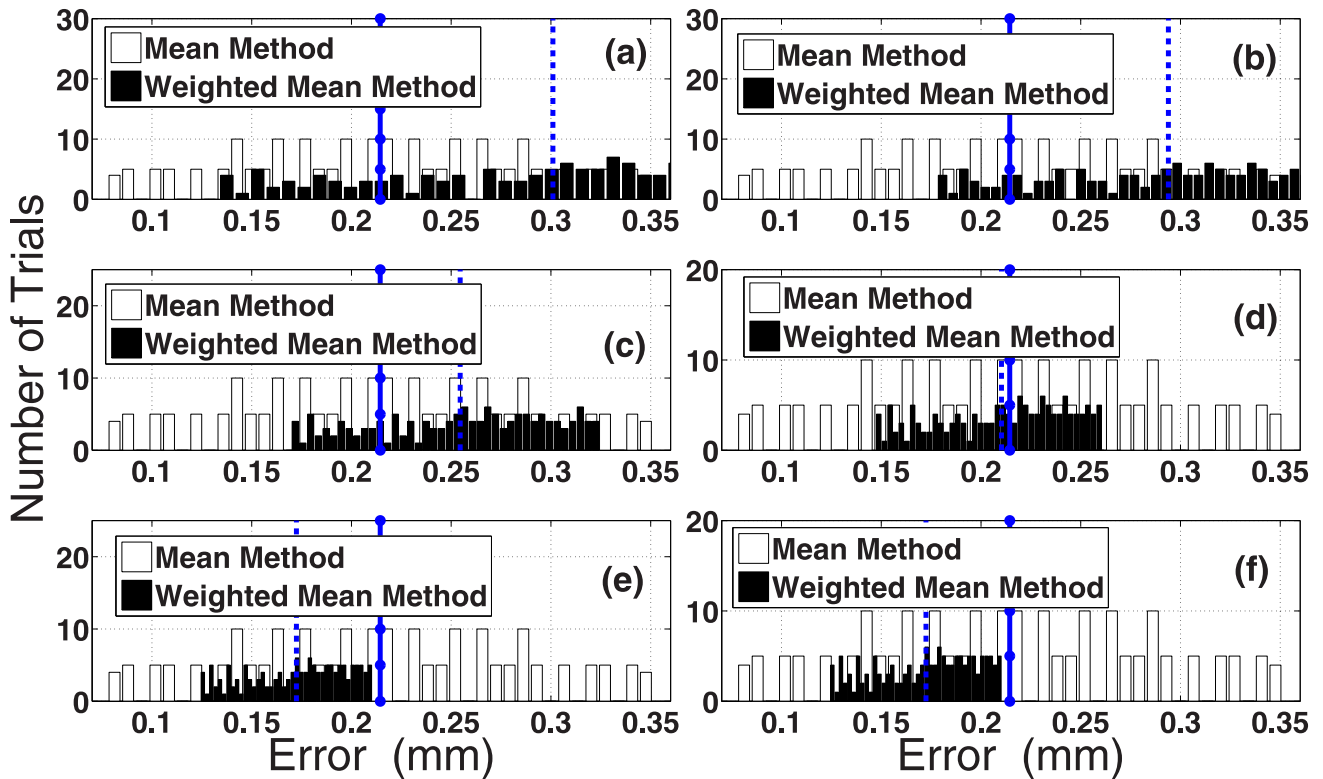


Figure 5. Histogram of the absolute error (in mm) for the mean method and the weighted mean method when processing the coseismic series between 5 and 9 yr [(a) 4.5 + 0.5 yr, (b) 4.5 + 1 yr, (c) 4.5 + 1.5 yr, (d) 4.5 + 2 yr, (e) 4.5 + 3 yr, (f) 4.5 + 4.5 yr]. Note that the (blue) dotted line is the mean value for the Mean method, the (blue) dashed line is the mean value for the Weighted Mean method.

coseismic offset can often benefit from long GPS time-series before the event occurs. For the mean method, long GPS time-series are not really useful, except to remove the tectonic rate more accurately.

Our previous results show that the more data available, the more precise and accurate is the estimated coseismic offset when using the weighted mean method. Let us fix a certain amount of data before an event to be equal to 4.5 yr. We call this realistic case ‘asymmetric GPS time-series’ to differ from the symmetric GPS time-series used until now. We then do a similar processing as described in Section 3.2.1 to estimate the distribution of the absolute error in the asymmetric case, except that we vary the amount of data after the date of the event from 6 months (or 4.5 + 0.5 yr) to 4.5 yr (4.5 + 4.5 yr). Fig. 5 shows the histogram of the absolute error in the coseismic offset estimates. The mean and standard deviation values are displayed in Appendix B. With 1.5 yr of data the two methods are comparable in terms of mean value of the error, but the standard deviation of the results is almost 50 per cent less than the one associated with the mean method. With at least 2 yr of post-event data, the weighted mean method estimate more accurately the coseismic offsets than the mean method.

3.3 Application to Sumatra–Andaman earthquake

This section deals with the question on the amount of data required to get a precise and accurate displacement field produced by the Sumatra–Andaman earthquake (2004 December 26), giving an estimation on how long we needed to wait after this event.

3.3.1 GPS processing and methodology

We processed GPS observations using the *GAMIT/GLOBK* software (Herring *et al.* 2010) as three interwoven global subnetworks of 20 sites, each with at least five common sites between the subnetworks. This is similar to the processing described in Tregoning & Watson (2009) and repeated in Montillet *et al.* (2013a). We used the *VMF1* mapping function and zenith hydrostatic delay from the *ECMWF* numerical model (Boehm *et al.* 2006). The loosely constrained daily subnetworks were combined in a second step where the terrestrial reference frame was defined by performing a six-parameter Helmert transformation of the coordinates of 20 sites into the *ITRF2008* (Altamimi *et al.* 2011). The steps undertaken to realize the reference frame were identical for all solutions. Finally, the GPS time-series are 9.5 yr long (2000 March–2010 January). Note that in the following study, we selected only 21 sites around the epicentre of the Sumatra–Andaman earthquake as displayed in Fig. 7.

Following previous sections (in particular Section 3.2.2), the tectonic rate is removed from the GPS coordinate time-series before applying the mean method. Thus, the mean method is used with a maximum of data equal to 100 d (50 d before and after the event). Note that if we could detect an optimum window or other events occurring in the selected amount of data, then we reduced it further.

Moreover, we estimated coseismic offsets due to large events ($M_w > 7.8$) occurring during the period 2000–2009 and then corrected the GPS time-series before calculating the coseismic offset series for our nominated event associated with the weighted mean method. The list of earthquakes includes the Hokkaido (2003

September 25), Macquarie Ridge (2004 December 23), Northern Sumatra (2005 March 28), Tonga (2006 May 3), Solomon Islands (2007 April 1), Southern Sumatra (2007 September 12) and Samoa (2009 September 29). As shown in Section 3.1 (e.g. Scenario 2), this approach should limit the influence of additional events when estimating the coseismic offset of the main event. The list of those world-wide earthquakes is provided by the Global CMT Catalogue (Ekström *et al.* 2012). Note that we do not show the results for GPS stations in the near-field of the Sumatra–Andaman earthquake (e.g. *SAMP*) as this work focuses only on stations in the far-field of an event. Following the studies of Watson *et al.* (2010) and Tregoning *et al.* (2013), we also discard the GPS stations which were strongly offset by the Macquarie Ridge earthquake (2004 December 23) which had a magnitude equal to $M_w \simeq 8$ (e.g. *AUCK*, *DUNT*, *CHAT*, *MAC1*, *HOB2*, *TIDB* and *MOBS*).

Finally, the predicted displacement field using an updated version of the spherical elastic model developed by Pollitz (1996) is also shown in Fig. 7 (red arrows), in order to do a comparison with the results using our methods. The parameters to model the Sumatra–Andaman earthquake are exactly the same as the values of Pollitz *et al.* (2006). The estimated values are the same as in Tregoning *et al.* (2013) and displayed in Appendix C.

3.3.2 Long time-series: How long do we need to wait with the weighted mean method to get almost the same coseismic estimates as with 9 yr of data?

Following the beginning of this section, we fix the amount of data before the date of the event equal to 4.5 yr, and we vary the amount of data available after this date. Let us process the coseismic offset series for 21 stations situated in the far-field of the Sumatra–Andaman earthquake with the weighted mean method. If we then assume that a total of 9 yr of GPS data is enough to calculate accurately a coseismic offset in the far-field of an event, one can wonder how many years are required to get similar coseismic offset estimates and uncertainties with an acceptable small error. We define the ratio of the estimated coseismic offset on the east and north coordinates as:

$$ratio = \frac{1}{2} \left[\left| \frac{C_e(L)}{U_e(L)} - \frac{C_e(9)}{U_e(9)} \right| + \left| \frac{C_n(L)}{U_n(L)} - \frac{C_n(9)}{U_n(9)} \right| \right] \quad (6)$$

with $|\cdot|$ the absolute value, $C_e(L)$ and $C_n(L)$ the estimated coseismic offset on the east and north coordinates with L years of data; $U_e(L)$ and $U_n(L)$ the corresponding uncertainties on the east and north coordinates with L years of data. The general idea of this ratio is to have a quantitative measure to compare the estimated coseismic offset associated with the uncertainty with 9 (4.5 + 4.5) yr of data and less (i.e. 4.5 + 2.5 yr). The smaller the ratio is, the more similar the estimated coseismic offsets with 9 yr and L years are. The ratio can also be interpreted in terms of the angle between two vectors (defined by the east and north coordinates).

In order to get the vectors of field displacement formed by the coseismic offset estimated on the east and north coordinates using L years and 9 yr of GPS data almost co-linear, meaning that the angle between the two vectors should be smaller than 5° , we are calculating the percentage of stations with a ratio smaller than a threshold chosen from 1 to 4 (1 corresponds to an angle smaller than 2° or an error smaller than 0.5 mm; 4 is an angle smaller than 5° and error smaller than 2 mm). These values correspond to a mean error between the estimated coseismic offsets ranging from 0.3 to 2 mm. Fig. 6 shows the results. Over all, one can see that between 2 and 3 yr of GPS data after the event are necessary to get more than 80 per cent of the total number of GPS stations when the threshold

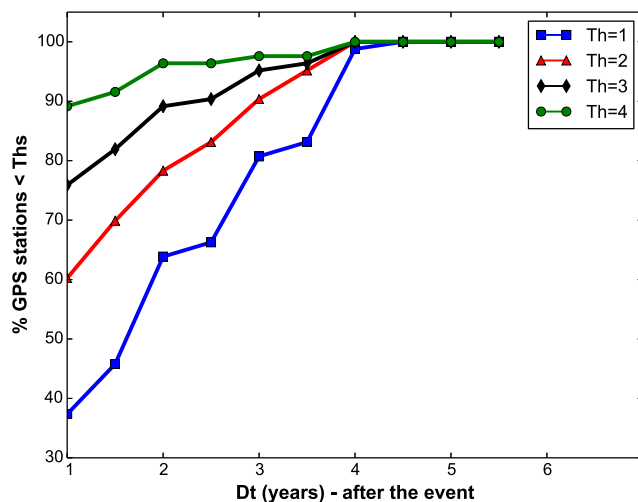


Figure 6. Graph of the percentage of GPS stations with a ratio defined in eq. (6) better than a given threshold (Ths) when varying the amount of data in order to estimate the coseismic offset with the weighted mean method (asymmetric series).

is bigger than 1. Otherwise, up to 4 yr of data are required. Finally, Fig. 7 shows the displacement field after the Sumatra–Andaman earthquake. We can compare the coseismic offset estimates with the weighted mean method (4.5 + 2.5 yr) and the results from Tregoning *et al.* (2013) (red arrows). We choose 2.5 yr of data after the event occurred according to the previous results. Overall, the results agree especially for the stations *CEDU*, *MAW1*, *PETP* and *YAR2* with the difference in the estimates (east and north) less than 0.5 mm. The estimated coseismic offsets are displayed in Table C1.

3.3.3 Estimation of the coseismic offset using the mean method and weighted mean method

Let us estimate the coseismic offset and uncertainties for 21 GPS stations situated in the far-field of the Sumatra–Andaman earthquake with the weighted mean method and the mean method with, respectively, 4.5 + 2.5 yr of data and 100 d. Fig. 7 shows the displacement field after applying the two methods. We can see that the weighted mean method produces generally larger coseismic offset vectors than the mean method. If we look at the absolute value of the ratio between the size of the coseismic vector and the size of the uncertainties displayed in Fig. 8, it shows that the standard deviation of the distribution over all GPS stations is the largest for the weighted mean method compared with the ratio of the estimates with the mean method. This supports that the uncertainties associated with the mean method are twice as large as those of the weighted mean method. Thus, the estimates with the mean method are likely to be less significant than the ones estimated with the weighted mean method. In other words, the weighted mean method is producing more statistically significant far-field coseismic estimates when compared with the associated uncertainties over the whole displacement field shown in Fig. 7.

3.3.4 The effects of post-seismic relaxation on coseismic offset estimates

Post-seismic relaxation occurred after the Sumatra–Andaman earthquake (Kreemer *et al.* 2006b). The presence of such non-linear site

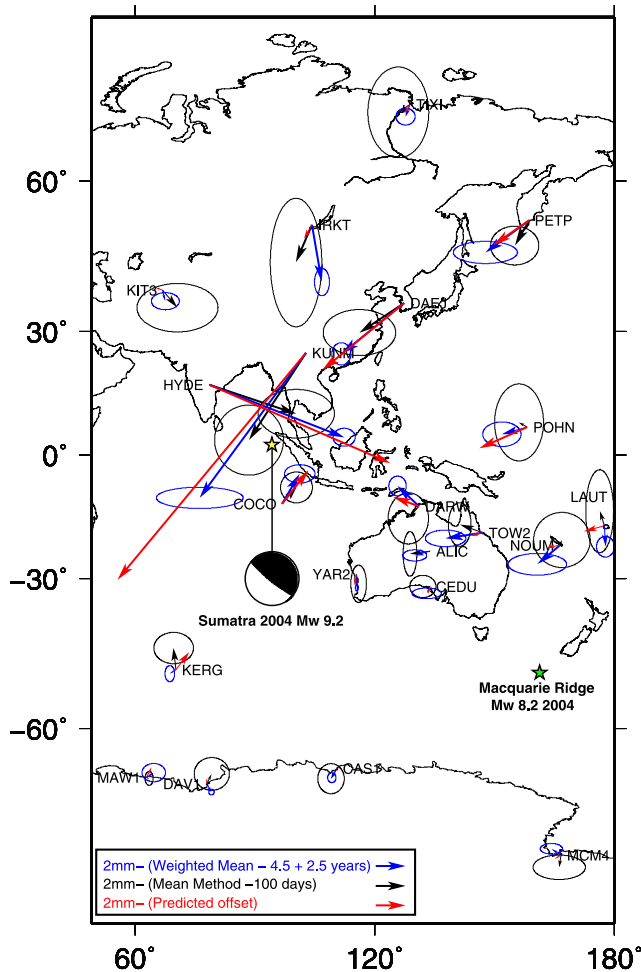


Figure 7. Estimated coseismic offsets (arrows) and uncertainties (ellipses) for 21 GPS stations in the far-field of the Sumatra–Andaman earthquake using the weighted mean method (4.5 + 2.5 yr, blue arrows) and the mean method (maximum 100 d, black arrows). Predicted offsets are estimated in Tregoning *et al.* (2013) (red arrows).

motion would affect the estimates of coseismic offsets, as shown in Figs 2(a) and (b). In order to ensure that our estimated far-field coseismic displacements shown in Fig. 7 are not affected by post-seismic relaxation, we enhanced our full method to include an exponential decay function, then estimated through a non-linear inversion the amplitude and time constant of the decay model along with our other parameters. We found statistically insignificant values for the amplitudes and the time constants. *F*-test results confirmed that these additional post-seismic relaxation parameters were not required, at the 95 per cent confidence limit in the model, confirming that our far-field estimates of coseismic displacement are not biased by the presence of post-seismic relaxation. On the other hand, we found significant amplitudes and time constants for the GPS site at Hobart, corresponding to the Macquarie Ridge earthquake (2004 December 23). This confirms previous evidence of post-seismic relaxation occurring on the southeast coast of Australia after this earthquake (Watson *et al.* 2010; Tregoning *et al.* 2013).

4 CONCLUSION

We develop a way to estimate precisely and accurately small coseismic offsets in the far-field of an earthquake based on the statistical

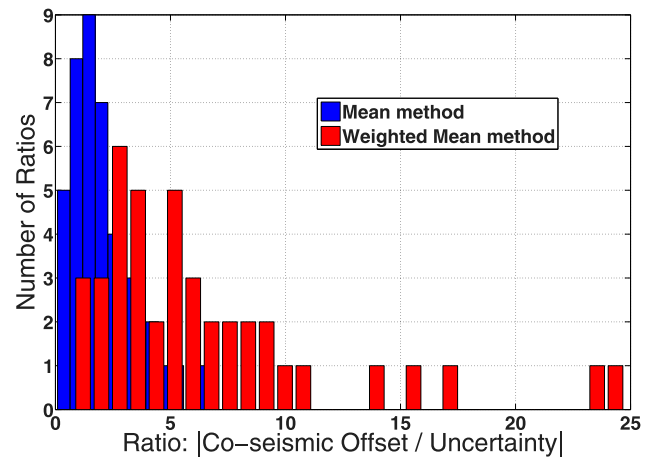


Figure 8. Histogram of the absolute value of the ratio of the estimated coseismic offsets and their associated uncertainties (east and north coordinates) for 21 GPS stations in the far-field of the Sumatra–Andaman earthquake. The coseismic offsets are estimated with the weighted mean method with 4.5 + 2.5 yr (red) and the mean method with 100 d (blue) of GPS data.

analysis of a coseismic offset series. This series is produced either by averaging GPS coordinates immediately preceding and following the day of an event (mean method), or using the least-squares technique with a complete site motion to model the GPS coordinate time-series, including a tectonic rate and seasonal variations. From the coseismic offset series produced with the complete site motion model, the final estimate is calculated with a weighted mean method.

With simulated GPS time-series and theoretical analysis, we show that the key point with the mean method to obtain precise and accurate results is to estimate a coseismic offset by finding an inflection point in the coseismic offset series. In addition, the results underline a greater sensitivity (large uncertainties) of this method than the weighted mean method in the presence of large amplitude geophysical processes and stochastic processes. With a large amount of data (at least 1000 d before and after the event), the coseismic offset series, resulting from using a complete site motion model including seasonal variations, is asymptotic to the true value of the coseismic offset when the seasonal signal is simulated with a deterministic model in the GPS time-series. However with a non-stochastic model of the seasonal signal in the simulated GPS time-series (i.e. GRACE elastic deformation signal), the coseismic offset estimate is biased by up to 0.5 mm for an amplitude of the seasonal signal greater than 1 mm.

We used our full method to compute far-field coseismic displacements associated with the Sumatra–Andaman earthquake using 9-yr GPS time-series for 21 stations in the far-field of the earthquake, we show that 2–3 yr after the Sumatra–Andaman event are necessary to have at least 80 per cent of all the stations with coseismic offset estimates and uncertainties comparable to the estimates produced using all available data. Statistically significant far-field coseismic estimates extend as far as 5500 km from the fault rupture zone using the weighted mean method.

The weighted mean method should be used to estimate accurately and precisely coseismic offsets in the far-field of an event when 2–3 yr of post-event data are available. With less GPS data available, one can use the mean method, which generally produces large uncertainties, and thus less statistically significant estimated coseismic offsets. While each GPS time-series is a unique sum of stochastic and geophysical processes, it is possible to decrease the

sensitivity of the mean method to these signals through a careful analysis of the coseismic offset series.

ACKNOWLEDGEMENTS

This research is supported by the Australian Research Council grant number DP0877381. The authors want to thank Dr Paul Tregoning, Dr Kevin Fleming, Dr Herb McQueen and the anonymous reviewers for their comments to improve the manuscript. GPS data used in this study are available at the SOPAC RINEX archive (sopac.ucsd.edu).

REFERENCES

- Altamimi, Z., Collilieux, X. & Métivier, L., 2011. ITRF2008: an improved solution of the international terrestrial reference frame, *J. Geod.*, **85**(8), 457–473.
- Banerjee, P., Pollitz, F.F. & Burgmann, R., 2005. The size and duration of the Sumatra-Andaman earthquake from far-field static offsets, *Science*, **308**, 1769–1772.
- Banerjee, P., Pollitz, F.F., Nagarajan, B. & Burgmann, R., 2007. Coseismic slip distributions of the 26 December 2004 Sumatra-Andaman and 28 March 2005 Nias earthquakes from GPS static offsets, *Bull. seism. Soc. Am.*, **97**, doi:10.1785/0120050609.
- Bevis, M., Scherer, W. & Merrifield, M., 2002. Technical issues and recommendations related to the installation of continuous GPS stations at tide gauges, *Mar. Geod.*, **25**, doi:10.1080/014904102753516750.
- Blewitt, G. & Lavallée, D., 2002. Effect of annual signals on geodetic velocity, *J. geophys. Res.*, **107**, B2145, doi:10.1029/2001JB000570.
- Boehm, J., Werl, B. & Schuh, H., 2006. Troposphere mapping functions for GPS and very long baseline interferometry from European Centre for Medium-Range Weather Forecasts operational analysis data, *J. geophys. Res.*, **111**, B02406, doi:10.1029/2005JB003629.
- Boschi, E., Casarotti, E., Devoti, R., Melini, D., Piersanti, A., Pietrantonio, G. & Riguzzi, F., 2006. Coseismic deformation induced by the Sumatra earthquake, *J. Geodyn.*, **42**(1–3), 52–62.
- Bürgmann, R., Ergintav, S., Segall, P., Hearn, E.H., McClusky, S., Reilinger, R.E., Woith, H. & Zschau, J., 2002. Time-space variable afterslip on and deep below the Izmit earthquake rupture, *Bull. seism. Soc. Am.*, **92**, 126–137.
- Chen, H.Y., Kuo, L.C. & Yu, S.B., 2004. Coseismic movement and seismic ground motion associated with the 31 March 2002 Hualien 331 earthquake, *Terr. Atmos. Ocean. Sci.*, **15**(4), 683–695.
- Darbeheshhti, N., Zhou, L., Tregoning, P., McClusky, S. & Purcell, A., 2013. The ANU GRACE visualisation web portal, *Comput. Geosci.*, **52**, 227–233.
- Davis, J.L.B., Wernicke, P. & Tamisiea, M.E., 2012. On seasonal signals in geodetic time series, *J. geophys. Res.*, **117**, B01403, doi:10.1029/2011JB008690.
- Ekström, G., Nettles, M. & Dziewonski, A.M., 2012. The global CMT project 2004–2010: Centroid-moment tensors for 13,017 earthquakes, *Phys. Earth planet. Inter.*, **200–201**, doi:10.1016/j.pepi.2012.04.002.
- Gazeaux, J. et al., 2013. Detecting offsets in GPS time series: First results from the detection of offsets in GPS experiment, *J. geophys. Res.*, **118**(5), 2397–2407.
- Herring, T.A., King, R.W. & McClusky, S.C., 2010. Introduction to GAMIT/GLOBK, Report, Mass. Inst. of Technol., Cambridge.
- Khan, S.A. & Gudmundsson, O., 2005. GPS analysis of the Sumatra-Andaman earthquake, *EOS, Trans. Am. geophys. Un.*, **86**, 89–94.
- Kreemer, C., Blewitt, G., Hammond, W.C. & Plag, H.-P., 2006a. Global deformation from the Great 2004 Sumatra-Andaman earthquake observed by GPS: Implications for the rupture process and global reference frame, *Earth Planets Space*, **58**, 141–148.
- Kreemer, C., Blewitt, G. & Maerten, F., 2006b. Co- and postseismic deformation of the 28 March 2005 Nias Mw 8.7 earthquake from continuous GPS data, *Geophys. Res. Lett.*, **33**, L07307, doi:10.1029/2005GL025566.
- Larson, K.M. & Agnew, D.C., 1991. Application of the Global Positioning System to crustal deformation measurement, 1. Precision and accuracy, *J. geophys. Res.*, **96**, doi:10.1029/91JB01275.
- Mahnke, R., Kaupuz, J. & Lubashevsky, I., 2008. *Physics of Stochastic Processes*, 1st edn, Wiley.
- Milne, G.A., Davis, J.L., Mitrovica, J.X., Schenrneck, H.-G., Johansson, J.M., Vermeer, M. & Koivula, H., 2001. Space-geodetic constraints on glacial isostatic adjustment in Fennoscandia, *Science*, **291**, 2381–2385.
- Montillet, J.P., Tregoning, P., McClusky, S. & Yu, K., 2013a. Extracting white noise statistics in GPS coordinate time series, *IEEE Geosci. Remote Sens. Lett.*, **10**(3), 563–567.
- Montillet, J.P., McClusky, S. & Yu, K., 2013b. Extracting colored noise statistics in time series via Negentropy, *IEEE Signal Process. Lett.*, **20**(9), 857–860.
- Plag, H.-P., Blewitt, G., Kreemer, C. & Hammond, W.C., 2006. Solid Earth deformations induced by the Sumatra earthquakes of 2004–2005: GPS detection of co-seismic displacements and tsunami-induced loading, in *Dynamic Planet – Monitoring and Understanding a Dynamic Planet with Geodetic and Oceanographic Tools*, Vol. 130, pp. 549–556, eds Tregoning, P. & Rizos, C. International Association of Geodesy Symposia, Springer-Verlag.
- Pollitz, F.F., 1996. Coseismic deformation from earthquake faulting on a layered spherical earth, *Geophys. J. Int.*, **125**, 1–14.
- Pollitz, F.F., Burgmann, R. & Banerjee, P., 2006. Post-seismic relaxation following the great 2004 Sumatra-Andaman earthquake on a compressible self-gravitating Earth, *Geophys. J. int.*, **167**, doi:10.1111/j.1365-246X.2006.03018.x.
- Tregoning, P. & Watson, C., 2009. Atmospheric effects and spurious signals in GPS analyses, *J. geophys. Res.*, **114**, B09403, doi:10.1029/2009JB006344.
- Tregoning, P., Watson, C., Ramilien, G., McQueen, H. & Zhang, J., 2009. Detecting hydrologic deformation using GRACE and GPS, *Geophys. Res. Lett.*, **36**, doi:10.1029/2009GL038718.
- Tregoning, P., Burgette, R., McClusky, S.C., Lejeune, S., Watson, C.S. & McQueen, H., 2013. A decade of horizontal deformation from great earthquakes, *J. geophys. Res.*, **118**, doi:10.1002/jgrb.50154.
- Watson, C., Burgette, R., Tregoning, P., White, N., Hunter, J., Coleman, R., Handsworth, R. & Broisma, H., 2010. Twentieth Century constraints on sea level change and earthquake deformation at Macquarie Island, *Geophys. J. Int.*, **182**(2), 781–796.
- Wdowinski, S., Bock, Y., Zhang, J., Fang, P. & Genrich, J., 1997. Southern California Permanent GPS geodetic array: Spatial filtering of daily positions for estimating coseismic and postseismic displacements induced by the 1992 Landers earthquake, *J. geophys. Res.*, **102**(B8), 18 057–18 070.
- Williams, S.D.P., 2003a. The effect of coloured noise on the uncertainties of rates estimated from geodetic time series, *J. Geod.*, **76**, doi:10.1007/s00190-002-0283-4.
- Williams, S.D.P., 2003b. Offsets in Global Positioning System time series, *J. geophys. Res.*, **108**, doi:10.1029/2002JB002156.
- Williams, S.D.P., Bock, Y., Fang, P., Jamason, P., Nikolaidis, R.M., Prawirodirdjo, L., Miller, M. & Johnson, D.J., 2004. Error analysis of continuous GPS position time series, *J. geophys. Res.*, **109**, B03412, doi:10.1029/2003JB002741.

APPENDIX A: ADDITION TO SECTION 2.3

This section shows how to derive eqs (2) and (3). Following the notation given in Section 2.3, the formal covariance matrix for the estimated parameters. Formulating eq. (1) in matrix form:

$$\mathbf{y} = (y_0, \dots, y_{N-1})^T$$

$$\mathbf{A} = \begin{bmatrix} 1 & t_0 & p_0 \\ 1 & t_1 & p_1 \\ \vdots & \vdots & \vdots \\ 1 & t_{N-1} & p_{N-1} \end{bmatrix}$$

$$\hat{\mathbf{v}} = (\hat{y}_0, \hat{r}, \hat{o})^T. \quad (\text{A1})$$

The estimates of y_0 , r and o are obtained from the general formula:

$$\hat{\mathbf{v}} = [\mathbf{A}^T \mathbf{A}]^{-1} \mathbf{A}^T \mathbf{y}. \quad (\text{A2})$$

The covariance matrix for the estimates is given by

$$\hat{\mathbf{C}}_{\hat{\mathbf{v}}} = [\mathbf{A}^T \mathbf{A}]^{-1}. \quad (\text{A3})$$

$$\hat{\mathbf{v}} = [\mathbf{A}^T \mathbf{A}]^{-1} \mathbf{A}^T \mathbf{y}. \quad (\text{A4})$$

If we assume the time-series is of length T and the offset is in the middle of the time-series at $\frac{T}{2}$, when developing the expression of the design matrix \mathbf{A} the covariance matrix for the estimated parameters is:

$$\begin{aligned} \hat{\mathbf{C}}_{\hat{\mathbf{v}}} &= \sigma_{\text{wh}}^2 [\mathbf{A}^T \mathbf{A}]^{-1} \\ &\approx \sigma_{\text{wh}}^2 \Delta t \begin{pmatrix} \int_0^T dt & \int_0^T t dt & \int_{T/2}^T dt \\ \int_0^T t dt & \int_0^T t^2 dt & \int_{T/2}^T t dt \\ \int_{T/2}^T dt & \int_{T/2}^T t dt & \int_{T/2}^T dt \end{pmatrix}^{-1} \end{aligned} \quad (\text{A5})$$

which can be shown to be equal to:

$$\hat{\mathbf{C}}_{\hat{\mathbf{v}}} \approx \sigma_{\text{wh}}^2 \Delta t \begin{pmatrix} T & \frac{T^2}{2} & \frac{T}{2} \\ \frac{T^2}{2} & \frac{T^3}{3} & \frac{3T^2}{8} \\ \frac{T}{2} & \frac{3T^2}{8} & \frac{T}{2} \end{pmatrix}^{-1} = \sigma_{\text{wh}}^2 \Delta t \begin{pmatrix} \frac{5}{T} & \frac{-12}{T^2} & \frac{4}{T} \\ \frac{-12}{T^2} & \frac{48}{T^3} & \frac{-24}{T^2} \\ \frac{4}{T} & \frac{-24}{T^2} & \frac{16}{T} \end{pmatrix}. \quad (\text{A6})$$

The equation for the bias in the offset becomes:

$$\sigma_{\hat{o}(\text{wh})} \approx \sqrt{\frac{16\sigma_{\text{wh}}^2 \Delta T}{T}} \quad (\text{A7})$$

As the data interval decreases the least squares estimate can be shown to converge to

$$\hat{\mathbf{v}} = \begin{pmatrix} \int_0^T A_1(t)^2 dt & \int_0^T A_1(t)A_2(t) dt & \int_0^T A_1(t)A_3(t) dt \\ \int_0^T A_1(t)A_2(t) dt & \int_0^T A_2(t)^2 dt & \int_0^T A_2(t)A_3(t) dt \\ \int_0^T A_3(t)A_1(t) dt & \int_0^T A_3(t)A_2(t) dt & \int_0^T A_3(t)^2 dt \end{pmatrix}^{-1} \begin{pmatrix} \int_0^T A_1(t)y(t) dt \\ \int_0^T A_2(t)y(t) dt \\ \int_0^T A_3(t)y(t) dt \end{pmatrix}, \quad (\text{A8})$$

where

$$A_1(t) = 1$$

$$A_2(t) = t$$

$$A_3(t) = p_i(t_{\text{off}}),$$

where $p_i(t_{\text{off}})$ is the Heaviside step function at the time of the offset, t_{off} . Now if $y(t)$ is some function that we have failed to take into account of then it will produce a bias in the estimates $\hat{\mathbf{v}}$ which we can calculate using eq. (A8). So we can substitute $y(t) = a \cos(2\pi ft - \phi)$ into

eq. (A8) such that the right-hand vector becomes:

$$\begin{pmatrix} \int_0^T A_1(t)y(t) dt \\ \int_0^T A_2(t)y(t) dt \\ \int_0^T A_3(t)y(t) dt \end{pmatrix} = \begin{pmatrix} \int_0^T a \cos(2\pi ft - \phi) dt \\ \int_0^T a t \cos(2\pi ft - \phi) dt \\ \int_{T/2}^T a \cos(2\pi ft - \phi) dt \end{pmatrix} = \begin{pmatrix} \frac{a}{2\pi f}(\sin(\phi) - \sin(\phi - 2\pi Tf)) \\ \frac{a}{4\pi^2 f^2}(\cos(\phi - 2\pi Tf) - \cos(\phi) - 2\pi Tf \sin(\phi - 2\pi Tf)) \\ \frac{a}{2\pi f}(\sin(\phi - \pi Tf) - \sin(\phi - 2\pi Tf)) \end{pmatrix}. \quad (\text{A9})$$

If we expand the equations we get the offset bias equal to:

$$\hat{\sigma}(T, \phi) = \frac{2a}{\pi^2 T^2 f^2} (3 \cos(\phi) - 3 \cos(\phi - 2\pi Tf) + \pi Tf(4 \sin(\phi - \pi Tf) + \sin(\phi - 2\pi Tf) + \sin(\phi))). \quad (\text{A10})$$

Clearly this is a function of T and ϕ . To quantify the offset bias as a rms, we need to average the equation over all possible phase lags.

$$\begin{aligned} \sigma_{\hat{\sigma}}(T) &= \left(\frac{1}{2\pi} \int_0^{2\pi} \hat{\sigma}^2(T, \phi) d\phi \right)^{1/2} \\ &= \frac{2a}{(\pi Tf)^2} (9 - 9 \cos(2\pi Tf) - 6\pi Tf(4 \sin(\pi Tf) + \sin(2\pi Tf)) + 2(\pi Tf)^2 (\cos(\pi Tf + 2))^2)^{1/2} \end{aligned} \quad (\text{A11})$$

That is eq. (3).

Now, if we apply the same methodology to estimate the coseismic offset bias with the least-squares when not accounting for a post-seismic relaxation mechanism [$y_p(t, \tau) = B(1 - \exp(-\frac{t}{\tau}))$], we end up with:

$$\begin{pmatrix} \int_{T/2}^T A_1(t)y_p(t, \tau) dt \\ \int_{T/2}^T A_2(t)y_p(t, \tau) dt \\ \int_{T/2}^T A_3(t)y_p(t, \tau) dt \end{pmatrix} = \begin{pmatrix} \int_{T/2}^T B(1 - \exp(-\frac{t}{\tau})) dt \\ \int_0^T t B(1 - \exp(-\frac{t}{\tau})) dt \\ \int_{T/2}^T B(1 - \exp(-\frac{t}{\tau})) dt \end{pmatrix} = \begin{pmatrix} L_1(T, \tau) \\ L_2(T, \tau) \\ L_1(T, \tau) \end{pmatrix} = \begin{pmatrix} B(\frac{T}{2} + \tau \exp(-\frac{T}{\tau}) (1 - \exp(\frac{T}{2\tau}))) \\ B(\frac{3T^2}{8} + \tau T \exp(-\frac{T}{\tau}) (1 - \frac{1}{2} \exp(\frac{T}{2\tau}))) \\ + \tau^2 \exp(-\frac{T}{\tau}) (1 - \exp(\frac{T}{2\tau})) \\ B(\frac{T}{2} + \tau \exp(-\frac{T}{\tau}) (1 - \exp(\frac{T}{2\tau}))) \end{pmatrix}. \quad (\text{A12})$$

By expanding the equations above, we find eq. (4).

Now in order to derive eq. (5), one can write the mean method such as:

$$\begin{aligned} \sigma_{\hat{\sigma}_2} &= \frac{2}{T} \int_{\frac{T}{2}}^T [rt + a \cos(2\pi ft - \phi) + y_p(t, \tau)] dt - \frac{2}{T} \int_0^{\frac{T}{2}} [rt + a \cos(2\pi ft - \phi)] dt \\ \sigma_{\hat{\sigma}_2} &= \frac{2}{T} \left[\int_{\frac{T}{2}}^T rt dt - \int_0^{\frac{T}{2}} rt dt \right] + \frac{2}{T} \left[\int_{\frac{T}{2}}^T a \cos(2\pi ft - \phi) dt - \int_0^{\frac{T}{2}} a \cos(2\pi ft - \phi) dt \right] + \frac{2}{T} \int_{\frac{T}{2}}^T [y_p(t, \tau)] dt \\ \sigma_{\hat{\sigma}_2} &= \sigma_1(T) + \sigma_2(T) + \sigma_3(T, \tau). \end{aligned} \quad (\text{A13})$$

By estimating $\sigma_1(T)$, $\sigma_2(T)$ and $\sigma_3(T)$, we end up with the results in eq. (5). Note that the contribution to the offset bias due to the seasonal variations [$\sigma_2(T)$] is averaged over ϕ (e.g. eq. 3).

APPENDIX B: ADDITION TO SECTION 3.2

These two Tables B1 and B2 display the mean and standard deviation values for Figs 4 and 5.

Table B1. Mean (μ) and standard deviation (σ) values for each histogram displayed in Fig. 4 for the Weighted Mean method and Mean method.

Scenarios	Weighted Mean m.		Mean m.	
	μ (mm)	σ (mm)	μ (mm)	σ (mm)
a	0.272	0.053	0.211	0.072
b	0.293	0.049	0.211	0.072
c	0.321	0.029	0.211	0.072
d	0.251	0.019	0.211	0.072
e	0.205	0.014	0.211	0.072
f	0.202	0.013	0.211	0.072

Table B2. Mean (μ) and standard deviation (σ) values for each histogram displayed in Fig. 5 for the Weighted Mean method and Mean method.

Scenarios	Weighted Mean m.		Mean m.	
	μ (mm)	σ (mm)	μ (mm)	σ (mm)
a	0.301	0.086	0.211	0.072
b	0.293	0.062	0.211	0.072
c	0.251	0.044	0.211	0.072
d	0.211	0.032	0.211	0.072
e	0.172	0.025	0.211	0.072
f	0.171	0.025	0.211	0.072

APPENDIX C: ADDITION TO THE SECTION 3.3

This Table C1 displays the values of the coseismic offset estimated with the weighted mean method (4.5 + 2.5 yr) shown in Fig. 7.

Table C1. Coseismic offset estimated with the weighted mean method (4.5 + 2.5 yr) at 21 stations in the far-field of the Sumatra–Andaman event. The last two columns (*E*ast and *N*orth) are the predicted offsets from Tregoning *et al.* (2013).

Station ID	Long. (°)	Lat. (°)	East (mm)	North (mm)	Unc. East (mm)	Unc. North (mm)	<i>E</i> ast (mm)	<i>N</i> orth (mm)
ALIC	133.89	−23.67	−1.03	−0.28	0.33	−0.15	0.01	0.05
CAS1	110.52	−66.28	−0.39	−0.69	0.12	0.11	−0.09	−0.05
CEDU	133.81	−31.87	−0.21	−0.45	0.39	0.14	−0.13	−0.52
COCO	96.83	−12.20	1.17	2.00	0.42	0.25	1.78	2.25
DAEJ	127.37	36.39	−4.20	−3.41	0.26	0.30	−5.46	−4.47
DARW	131.13	−12.84	−1.44	1.37	0.24	0.27	−1.73	0.62
DAV1	77.97	−68.58	0.29	−0.55	0.07	0.08	0.00	0.37
HYDE	78.55	17.42	8.26	−2.16	0.85	0.24	12.11	−5.24
IRKT	104.32	52.21	0.66	−3.82	0.20	0.37	−0.52	−0.92
KERG	70.25	−49.35	−0.42	−0.26	0.13	0.22	0.87	1.16
KIT3	66.88	39.13	0.18	−0.74	0.38	0.23	−0.51	0.18
KUNM	102.80	25.03	−7.11	−9.70	1.18	0.29	−12.59	−15.17
LAUT	177.45	−17.61	0.08	−1.39	0.24	0.28	−1.37	−0.37
MAW1	62.87	−67.60	0.47	0.30	0.32	0.25	0.34	0.68
MCM4	166.67	−77.83	−0.65	0.42	0.30	0.144	−0.44	−0.26
NOUM	166.41	−22.27	−1.52	−1.27	0.80	0.29	−0.91	−0.17
PETP	158.61	53.07	−2.91	−2.14	0.88	0.30	−2.41	−1.66
POHN	158.21	6.959	−1.70	−0.48	0.52	0.34	−3.21	−1.42
TIXI	128.87	71.63	−0.31	−0.84	0.26	0.23	−0.39	−0.63
TOW2	147.06	−19.27	−2.49	−0.37	0.55	0.23	−0.82	−0.21
YAR2	115.35	−29.05	0.04	−0.91	0.03	0.09	−0.11	−0.77